Neurobiology of Disease

The ZIP3 Zinc Transporter Is Localized to Mossy Fiber Terminals and Is Required for Kainate-Induced Degeneration of CA3 Neurons

Milos Bogdanovic,[1] Hila Asraf,[1] Noa Gottesman,[1] Israel Sekler,[1] Elias Aizenman,[1,2] and Michal Hershfinkel[1]

[1]Department of Physiology and Cell Biology, and the Zlotowski Center for Neuroscience, Ben-Gurion University of the Negev, Faculty of Sciences, Beer-Sheva 84105, Israel, and [2]Department of Neurobiology and Pittsburgh Institute for Neurodegenerative Diseases, University of Pittsburgh School of Medicine, Pittsburgh, Pennsylvania 15261

Tight regulation of neuronal Zn^{2+} is critical for physiological function. Multiple Zn^{2+} transporters are expressed in the brain, yet their spatial distribution and distinct roles are largely unknown. Here, we show developmental regulation of the expression of Zn^{2+} transporters ZIP1 and ZIP3 in mouse hippocampal neurons, corresponding to previously described increase in neuronal vesicular Zn^{2+} during the first postnatal month. Rates of Zn^{2+} uptake in cultured mouse hippocampal neurons, monitored using FluoZin-3 fluorescence, were higher in mature neurons, which express higher levels of ZIP1 and ZIP3. Zn^{2+} uptake was attenuated by ~50% following silencing of either ZIP1 or ZIP3. Expression of both ZIP1 and ZIP3 was ubiquitous on somas and most neuronal processes in the cultured neurons. In contrast, we observed distinct localization of the transporters in mouse hippocampal brain, with ZIP1 predominantly expressed in the CA3 stratum pyramidale, and ZIP3 primarily localized to the stratum lucidum. Consistent with their localization, silencing of ZIP1 expression in vivo reduced Zn^{2+} uptake in CA3 neurons while ZIP3 silencing reduced Zn^{2+} influx into dentate gyrus (DG) granule cells in acute hippocampal slices. Strikingly, in vivo silencing of ZIP3, but not ZIP1, protected CA3 neurons from neurodegeneration following kainate-induced seizures. Our results indicate that distinct Zn^{2+} transporters control Zn^{2+} accumulation and toxicity in different neuronal populations in the hippocampus and suggest that selective regulation of Zn^{2+} transporters can prevent seizure induced brain damage.

Key words: neurodegeneration; seizure; zinc; zinc toxicity; zinc transporter

Significance Statement

Zinc plays a major role in neuronal function and its dysregulation is associated with neurodegeneration. Multiple zinc tran are expressed in neurons, yet little is known on their distinct roles. Here, we show that the plasma membrane ZIP1 and Z transporters are expressed on distinct neuronal populations in the CA3 region of the hippocampus. We show that ZIP1 m zinc influx into postsynaptic cells, while ZIP3 is responsible for zinc re-uptake from this synapse into dentate granule cells ther show that silencing of ZIP3, but not ZIP1, can rescue the postsynaptic cells from kainate-induced neurodegeneration gests that neuronal zinc toxicity and degeneration can be modulated by regulation of specific zinc transporters function.

Introduction

A large component of Zn^{2+} in the brain is localized to synaptic vesicles of excitatory synapses, most strikingly in the mossy fiber (MF) terminals of the hippocampal dentate gyrus (DG) granule cells (Frederickson et al., 1981, 1992; Frederickson and Danscher, 1990). MF terminals accumulate increasing amounts of vesicular Zn^{2+} during the first postnatal month (Slomianka and Geneser, 1997; Nitzan et al., 2002). Vesicular Zn^{2+} is released during physiological activity to modulate neurotransmission via interaction with postsynaptic neurotransmitter receptors, as well as activation of metabotropic zinc receptor (mZnR/GPR39) signaling (Besser et al., 2009; Saadi et al., 2012; Anderson et al., 2015; Gilad et al., 2015; Kalappa et al., 2015; Krall et al., 2021). Changes in intracellular Zn^{2+} levels can be also detected following its translocation into postsynaptic cells following synaptic release, or after intracellular liberation from

Received Apr. 29, 2021; revised Dec. 16, 2021; accepted Jan. 19, 2022.

Author contributions: M.B., E.A., and M.H. designed research; M.B., H.A., and N.G. performed research; M.B., H.A., and M.H. analyzed data; M.B., E.A., and M.H. wrote the first draft of the paper; M.B., I.S., E.A., and M.H. edited the paper; M.B., E.A., and M.H. wrote the paper.

This work was supported by the The U.S.-Israel Binational Science Foundation (BSF) and National Science Foundation (NSF) Grant NSF-IOS-BSF 1655480 (to E.A. and M.H.).

The authors declare no competing financial interests.

Correspondence should be addressed to Michal Hershfinkel at hmichal@bgu.ac.il.

https://doi.org/10.1523/JNEUROSCI.0908-21.2022

metal binding proteins, such as metallothioneins (Aizenman et al., 2000; Weiss and Sensi, 2000; Zhang et al., 2004; Sensi et al., 2011). Excessive accumulation of Zn^{2+} is neurotoxic (Zhang et al., 2007; Ji et al., 2019; Aizenman et al., 2020; Granzotto et al., 2020), and, as such, tight spatiotemporal regulation of neuronal Zn^{2+} is of fundamental importance to maintain neuronal integrity.

In addition to metallothioneins (Krężel and Maret, 2021), two families of Zn^{2+} transporters are responsible for intracellular Zn^{2+} distribution by mediating movement of this ion across cellular and organelle membranes (Kraft et al., 2021). The ZRT-IRT-like transporters (ZIP) of the SLC39A superfamily transport Zn^{2+} into the cytosol, while members of the ZnT, SLC30A superfamily of transporters, as well as TMEM163 (Styrpejko and Cuajungco, 2021), move the metal out of the cell or into membranous organelles. Of the 25 Zn^{2+} transporters (14 ZIPs, 10 ZnTs, and TMEM163), many are expressed in an organelle-, cell-, or tissue-specific manner (Gaither and Eide, 2001; Milon et al., 2001; Nitzan et al., 2002; Kambe et al., 2015). In neurons, ZnT3 is essential for sequestration of Zn^{2+} into synaptic vesicles, establishing the well-described pool of vesicular Zn^{2+} present in the MFs (Palmiter et al., 1996; Wenzel et al., 1997; McAllister and Dyck, 2017). Several ZIP transporters are present in neurons (Qian et al., 2011; Nishikawa et al., 2017), but their specific roles in Zn^{2+}-mediated cellular processes had not been well characterized. Mice lacking ZIP1 and ZIP3, which are ubiquitous cell membrane Zn^{2+} importers (Dufner-Beattie et al., 2005; Belloni-Olivi et al., 2009), exhibit lower neuronal loss in the CA1 hippocampal region following kainate-induced epileptic seizures (Qian et al., 2011). While this study pointed to an important role for Zn^{2+} uptake mechanisms in neuronal survival or death, it did not define the specific roles played by each of the two transporters. Indeed, despite their critical potential role in neurodegeneration, little is known about the specific localization and function of ZIP1 and ZIP3 in neurons. As such, we set out to determine whether ZIP1 and ZIP3 have distinct roles in neuronal Zn^{2+} uptake and whether they differentially affect degeneration and survival following injury. Our results indicate that ZIP1 and ZIP3 expression is developmentally regulated and that in the adult hippocampus, ZIP1 and ZIP3 are present in different strata and regulate Zn^{2+} transport in distinct neuronal populations. Further, we demonstrate that ZIP3, but not ZIP1, is involved in neuronal degeneration following epileptic seizures.

Materials and Methods

All experimental procedures involving animals were performed according to approved protocols and in accordance with the committee for Ethical Care and Use of Animal in Experiments at the Faculty of Health Sciences at Ben-Gurion University. Animals were housed on a 12/12 h light/dark cycle, at a temperature of 20–24°C and 30–70% relative humidity and were provided with mice chow and water ad libitum.

Primary hippocampal neuronal cultures

Primary hippocampal neurons were prepared from postnatal day (P)0 C57BL/6JRcc mouse neonates. Hippocampi were treated with papain (Worthington) and dissociated by mechanic pipetting in HBSS supplied with 20 mM HEPES (pH 7.4), and cells were seeded on 50 mg poly-D-lysin-coated coverslips (Ø12 mm) in 24-well plates at the density of 5×10^5 cells/ml (coverslip). During the initial 24 h, cells were cultured in neurobasal medium (Invitrogen), supplemented with 5% fetal bovine serum (FBS), 2% B-27, 1% Glutamax-100, and 40 µg/ml gentamicin, after which the medium was devoid of serum. To suppress glial growth, 5 µM cytosine b-D-arabinofuranoside (AraC) was added to the medium on days in vitro (DIV5). All cells were cultured in a humidified atmosphere of 5% CO_2 at 37°C.

Immunofluorescent labeling of primary hippocampal neuronal cultures

Cell-seeded coverslips were removed from growth media, washed with PBS and immediately fixed in 4% paraformaldehyde for 10 min at room temperature. Next, cells were permeabilized with 0.1% Triton X-100 in PBS (3 min) and blocking was performed with 5% normal goat serum in PBS (1 h) at room temperature. Cells were incubated with either rabbit polyclonal anti-ZIP1 or anti-ZIP3 antibody (Abcam #ab105416, #ab117568); some coverslips were co-incubated with guinea pig anti-TAU (SySy 314004) in blocking solution for 1 h at room temperature. Following extensive wash with PBS, cells were incubated with appropriate secondary antibodies (Alexa488-conjugated or Alexa594-conjugated goat anti-rabbit and Alexa594-conjugated goat anti-guinea pig, Jackson ImmunoResearch). Coverslips were then mounted with Fluoromount DAPI-containing mounting medium.

Immunofluorescent labeling of hippocampal tissue sections

Anesthetized (ketamine/xylazine) C57BL/6JRccHsd mice (1 or 14 d and 1–1.5 months old) were transcardially perfused with ice cold PBS and 4% paraformaldehyde. Brains were extracted and postfixed in the same fixative overnight at 4°C. Tissue was then washed with PBS, dehydrated with increasing series of ethanol, cleared with toluene and infiltrated with paraffin. Ten-micrometer paraffin sections were obtained on a rotary microtome. After heat induced antigen retrieval in 10 mM sodium citrate (95°C, 10 min), tissue sections were washed and blocked with 5% NGS, 0.01% Triton X-100 in PBS (blocking solution). For ZIP1/ZIP3 double immunolabeling, sections were incubated overnight at 4°C with primary anti-ZIP1 (Abcam ab105416), and then incubated with Alexa488 conjugated monovalent F(ab) Fragments of Affinity-Purified goat anti-rabbit secondary antibodies for 1 h at room temperature. Slices were subsequently incubated with ZIP3 primary antibody (Abcam ab117568) overnight at 4°C, and then incubated with Alexa 647 goat anti-rabbit antibody for 1 h at room temperature. Sections were mounted with Fluoromount DAPI-containing mounting medium. For colocalization of ZIP1 or ZIP3 with Calbindin, following the above deparaffinization, antigen retrieval and blocking, sections were incubated with either rabbit anti-ZIP1 or ZIP3 (Abcam ab105416, ab117568) primary antibody mixed with mouse anti-Calbindin (Swant D-28K, 300) antibody overnight at 4°C, and with secondary antibodies (Alexa488-conjugated goat anti-mouse and Alexa594-conjugated goat anti-rabbit) as described above. For colocalization of ZIP3 and vesicular glutamate transporter 1 (Vglut1), following the above deparaffinization, antigen retrieval, sections were blocked with 5% normal horse serum, 0.01% Triton X-100 in PBS on room temperature for 1 h. Sections were then incubated with rabbit anti-ZIP3 and goat anti-Vglut1 (SySy, 135307) antibody overnight on 4°C, washed with PBS and incubated for 1 h at room temperature with a cocktail of Alexa488 conjugated donkey anti-goat and Alexa594 conjugated donkey anti-rabbit antibodies. Fluorescent images were acquired with appropriate filters using Nikon Eclipse Ti confocal microscope. Colocalization and overlap coefficients were calculated using ImageJ/Coloc2 plugin. Quantification of fluorescent signal measurements was performed in Adobe Photoshop, by averaging mean gray values of five randomly selected regions per hippocampal slice in stratum lucidum and in stratum pyramidale. For comparison, all data were normalized to mean values of the signal in the pyramidal layer for each age/transporter group.

Quantitative PCR (qPCR) analysis

For measuring mRNA levels of Zn^{2+} transporters in primary hippocampal neurons, cells were washed with PBS and homogenized using QIAshredder (QIAGEN) as suggested by the manufacturer. For hippocampal tissue measurements, hippocampi were dissected from wild-type (WT) mice of different ages following anesthesia with ketamine and xylazine and subsequent decapitation. Hippocampal tissue was dissociated and lysed in Lysis Buffer (Ambion, ThermoFisher Scientific) supplemented with b-mercaptoethanol. RNA was purified with

PureLink RNA Mini kit (Ambion, ThermoFisher Scientific) as described by the manufacturer and treated with DNase (Invitrogen). One microgram of purified RNA was converted to cDNA using Quanta cDNA synthesis kit as described by the manufacturer, which was then subjected to real-time PCR procedure (TaqmanApplied Biosystems). Primers and probes were supplied by Integrated DNA Technologies. The following sequences were used for the primers: ZIP1 forward primer, CTTGTAAGC CAGCGTGATCT and reverse primer, CTGCCATAGATGAGGCCTTG; ZIP3 forward primer, AGAAACCCACCATCATGAGC and reverse primer, CGTATTC CTGGCTA CATGCTT; ZIP12 forward primer, GTGAGTAAC AGTGCATCTGCT and reverse primer, CTCAAC CATCCACAA AGCCT; ZnT1 forward primer, TCCCATTTACTTGTACAT CCACTG and reverse primer, CCAACACCAGCAATTCCAAC; ZnT3 forward primer, GAGAATCCAAAC CGGGAATAGAG and reverse primer, TACTTACCACGTTGCCTCTG; ZnT10 forward primer, ACACCTCTGATATTGAGTGCTTC reverse primer, AC CGTGTTCTCTAATGTAGCAG; Actin forward primer, AGGTC TTTACGGATGTCAACG and reverse primer, ATTGGCAAC GAGCGGTT. Gene expression levels were normalized to actin and are presented as fold increase relative to the level in 3-d-old animals or DIV10 primary hippocampal neurons.

Generation of adeno-associated virus (AAV) particles for gene silencing
Gene transfer vectors based on AAV for expressing short hairpin RNA (shRNA) were used for targeted silencing of ZIP1 or ZIP3 transporters in vitro or in vivo. shRNA sequences for ZIP1, ZIP3 as well as scramble control were supplied by Transomic Technologies (control: sense 5′-ACACGT GTTGACAATTAATCAT-3′; shZIP1: sense 5′-CCCCCTT GCAAGAGTTCATCTA-3′; shZIP3: sense 5′-ACGGTGGCACCT TC CTGTTTGA-3′, all shRNAs contained TAGTGAAGC CACAGATGTA mir-30a loop). All the shRNA sequences were under the U6 promoter, preceded by the RFP gene under the human synapsin 1 gene promoter. Only RFP-positive cells were used for any experimental procedures involving the AAV-targeted silencing. For in vitro transduction, viral particles were prepared as described previously (Groh et al., 2008) in HEK-293T cells using both the pD1 and pD2 helper plasmids. For in vivo delivery, AAV-PHP.eB particles were produced as previously described (Challis, et al., 2019). Briefly, viral particles were harvested 72 h after transfection in HEK-293T cells, the cells were lysed (buffer containing 150 mM NaCl and 50 mM Tris) by three freeze-thaw cycles (37°C and 4°C) after which the buffer was incubated with 100 U/ml benzonase (Sigma, E1014) for 1 h at 37°C. This crude lysate was stored at 4°C and used for neuronal culture transduction. AAV-PHP.eB particles were purified for in vivo use by iodixanol (Optiprep, Sigma, D1556) gradient (15%, 25%, 40%, and 60%). Viruses were then concentrated using Amicon filters (EMD, UFC910024), and formulated in sterile PBS. Titer for each of the produced viruses was measured by determining the number of DNase I-resistant vg using qPCR. Finally, 1–2 × 10^9 vg were administered by intracranioventricular freehand injections of 2 μl per ventricle to cryoanesthetized P0/P1 littermate C57BL/6JRccHsd mouse neonates, at approximately half the distance between the eye and the lambda, as described previously (Kim et al., 2014). Subsequent experimental procedures were performed three or five weeks after injections for live tissue imaging or neurodegeneration assay, respectively.

Fluorescent Zn^{21} imaging in primary neuronal cultures
Live cell imaging was performed, as described (Ganay et al., 2015), on an Axiovert 100 inverted microscope (Zeiss) with 10 objective connected to Polychrome V monochromator (TILL Photonics) and fluorescence changes were recorded with SensiCam cooled charge-coupled camera (PCO) and measured with Imaging Workbench 5 (Indec). For silencing experiments, hippocampal cultures were transduced with viral vectors aimed to silence ZIP1 or ZIP3 or with a scramble control vector on DIV10. One week after transduction, cells were washed in physiological Ringer's solution (containing 120 mM NaCl, 5.4 mM KCl, 0.8 mM $MgCl_2$, 20 mM HEPES, 15 mM glucose, and 1.8 mM $CaCl_2$, at pH 7.4) and loaded with the cell permeant FluoZin-3 AM in Ringer's solution (1 μM, 30 min, room temperature). Cells were washed for 20 min after which the coverslips were mounted in a recording chamber on the imaging microscope. Cells were exposed to nominally Ca^{21}-free Ringer's solution for ;60 s to obtain baseline fluorescence level, followed by addition of 100 μM Zn^{21}. Fluorescence signal was recorded every 3 s and averaged over a minimum of 10 neurons (RFP-positive neurons for silencing experiments) for each coverslip. Traces are shown, and slopes of signal change were determined over initial 100 s, following addition of Zn^{21}. Averaged rates over n experiments are presented in the boxplots.

Fluorescent Zn^{21} imaging in acute hippocampal slices
Live tissue imaging was performed as described (Chorin et al., 2011) on an Olympus (IX-50) microscope with 10 water-immersed objective, connected to a Polychrome IV monochromator (TILL Photonics) and fluorescence changes were recorded with SensiCam cooled charge-coupled camera (PCO) and measured with Imaging Workbench 5 (Indec). Mouse C57BL/6JRcc neonates (P0–P1) were transduced with AAV-PHP.eB viral vectors aimed to silence ZIP3 or ZIP3 or scramble control vector, by intracranioventricular injections. Three weeks after transduction (P21), transverse brain slices (300 μm) were produced from animals of either sex. Acute slices were kept in continuously oxygenized artificial CSF (ACSF; 124 mM NaCl, 26 mM $NaHCO_3$, 1.25 mM NaH_2PO_4, 2 mM $MgSO_4$, 2 mM $CaCl_2$, 3 mM KCl, and 10 mM glucose, at pH 7.4) at room temperature for at least 1 h. For live imaging of cytosolic Zn^{21} changes, we used the cell permeant Zn^{21}-sensitive fluorescent dye, FluoZin-3. Slices were loaded with 1 μM FluoZin-3 AM in the presence of 0.02% pluronic acid, dissolved in ACSF, for 45 min (Gee et al., 2002; Chorin et al., 2011). Slices were incubated in fresh ACSF for additional 30 min, after which the slices were transferred to the recording chamber and mounted on the imaging microscope. To avoid Zn^{21} orthophosphate precipitates, during imaging the ACSF was changed to $NaPO_4$-free ACSF as previously done (Besser et al., 2009). For each brain slice, minimum of 10 RFP-positive neurons were selected, either in DG or CA3 hippocampal region, and baseline fluorescence was obtained (60 s) followed by addition of 200 μM Zn^{21}. Fluorescence signals were recorded every 3 s and fluorescence in each region of interest was normalized to its own baseline values. Traces are shown, and slopes of signal change were determined over initial 100 s. Averaged rates over n experiments are presented in the boxplots. For vesicular Zn^{21} measurements, slices were loaded with 30 μM Zinpyr1 (ZP1) for 30 min, which accumulates in vesicles (Burdette et al., 2001; Woodroofe et al., 2004), washed two times in ACSF, and rapidly transferred to the recording chamber. For each brain slice, minimum of 10 DG RFP-positive neurons were selected, and slices were superfused with ACSF for ;3 min to obtain baseline and then the membrane permeable Zn^{21} chelator TPEN (40 μM) was added. Fluorescence images were recorded every 30 s for the initial 5 min, to reduce bleaching images were acquired only every 150 s for 20 min, and finally for the last 5-min fluorescence was recorded every 30 s. Traces are shown, and fluorescence decrease was determined as a difference between the baseline and the final fluorescence intensity values. DTPEN, all presented as percentage of fluorescence decrease in control slices.

Neurodegeneration assay (Fluoro-Jade B and Nissl histochemistry)
Neonate C57BL/6JRcc mice (P0–P1) received intracranioventricular transduction of AAV vectors aiming to silence ZIP1 or ZIP3 or with scrambled control vector. Kainic acid (3 mg/ml) was administered five weeks later intraperitoneally to all animals in doses of 25–30 mg/kg and animals were continuously recorded to evaluate the seizure scores (using the following scale: grade 1, staring/unresponsive; grade 2, focal clonic convulsion, tail rigidity; grade 3, forelimb clonus with rearing into sitting position; grade 4, loss of posture broken by periods of total stillness; grade 5, continuous grade four seizures, status epilepticus; grade 6, body in clonus, as previously used; Gilad et al., 2015). Only animals that reached grade 5 (13 out of 15 animals, 4/5 animals in control or shZIP1, and 5/5 animals in shZIP3 group) were used for further immunohistochemical analysis. 30 min after initial grade 5 seizure all animals were treated with 10 mg/kg Diazepam to prevent further seizures and subsequent neurodegeneration. Animals were killed 24 h after the seizures (using ketamine/xylazine cocktail for anesthesia and perfusion with ice cold PBS and 4% paraformaldehyde). This protocol for early neurodegeneration following kainate administration was previously used to determine neuronal injury in ZIP1/ZIP3 double knock-out mice (Qian et al., 2011).

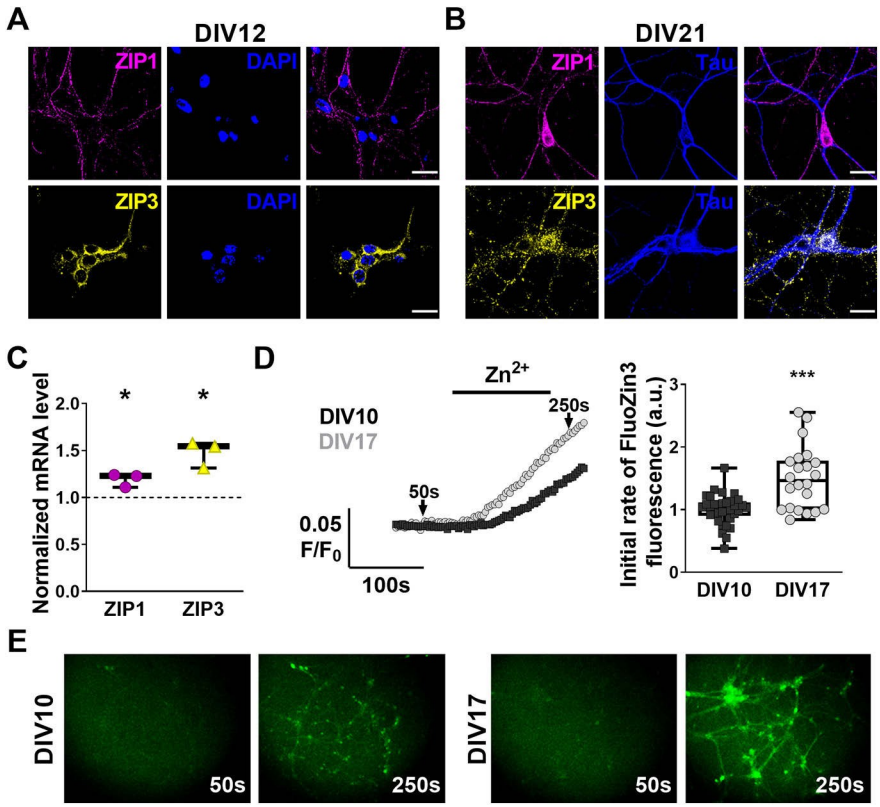

Figure 1. Increased ZIP1 and ZIP3 expression during maturation of primary hippocampal neurons. A, ZIP1 (upper, magenta) and ZIP3 (lower, yellow) immunofluorescent labeling of DIV12 primary hippocampal neurons. Somas are stained with DAPI (blue). B, ZIP1 (upper, magenta) and ZIP3 (lower, yellow) co-immunolabeling with the neuronal Tau (blue) of DIV21 primary hippocampal neurons. C, Analysis of mRNA expression levels of ZIP1 and ZIP3 in DIV17 hippocampal neurons compared with DIV10 (normalized to 1, shown as dotted line; n = 3 cultures per age group; $p < 0.05$, t test). D, Traces of FluoZin-3 fluorescence changes (left) in cultured hippocampal neurons exposed with 100 μM Zn^{2+} in Ringer's solution, added at the indicated time. Averaged initial slope of fluorescence rise (right), representing Zn^{2+} influx in hippocampal neurons (DIV10: n = 34 coverslips in 5 independent experiments; DIV17: n = 23 coverslips in 4 independent experiments; ***$p < 0.001$; using t test compared with DIV10). E, Representative images (10 magnification) of primary hippocampal neurons before (50 s, marked in D) and after (250 s) exposure to 100 μM Zn^{2+}-containing Ringer's solution, used for D. Cultures of DIV10 neurons shown in left panels and DIV17 neurons shown in right panels. Scale bar, 10 mm.

Importantly, relatively small but consistent cell death is observed in the hippocampus in this strain of mice in the latter studies, as well as in others (Schauwecker and Steward, 1997; McKhann et al., 2003; Schauwecker, 2003; Schauwecker et al., 2009). Our data show significant and consistent cell death at 24 h after kainate injection in all animals studied, as previously shown (McLin and Steward, 2006; Tzeng et al., 2013). Brains were harvested, postfixed in the same fixative overnight, and cryoprotected in 20% and 30% sucrose solutions. Finally, brains were embedded in Optimal cutting temperature compound (OCT) and frozen in liquid nitrogen. Twenty-micrometer coronal sections were obtained on a cryostat, mounted on gelatin coated glass slides and dried at room temperature overnight, and stored at 80°C. Neurodegeneration was assessed by Nissl (cresyl violet) staining and numbers of degenerating neurons were quantified using Fluoro-Jade B labeling (Millipore). Nissl staining and Fluoro-Jade B labeling were performed on serial sections for each animal. For Nissl staining, sections were washed and incubated in 50% 50% Chloroform/Methanol solution for 4 h at room temperature. Following incubation in descending series of ethanol and rehydration solutions, slides were incubated for 5 min in Nissl staining solution previously heated to 37°C. Excess dye was washed with brief rinse in water and distaining was performed with 95% ethanol until satisfactory level of staining was observed. Slides were dehydrated with absolute ethanol, cleared in xylene and mounted with DPX mounting medium. Neurodegeneration was observed as small apoptotic darker stained nuclei and regions of hippocampal tissue that showed loss of cellular elements or thickness of the specific region. For Fluoro-Jade B labeling, slides were washed and submerged in 80% ethanol, 1% NaOH for 5 min, and then in descending series of ethanol and rehydration solutions. Slides were then transferred to potassium permanganate 0.06% (in water) for 10 min, rinsed in water 1 min and incubated in 0.0004% Fluoro-Jade B in 0.1% acetic acid vehicle solution. Slides were cleared in xylene after absolute ethanol dehydration and mounted using DPX mounting medium. Quantification of Fluoro-Jade-positive (FJ^+) cells was performed on three to four brain sections, no less than 200 mm apart, per animal and averaged number of FJ^+ cells per section is shown in boxplots.

Statistical analysis

Unless otherwise stated, all data are shown in box and whisker plots with all data points and max-min value bars, number of mice used for each experiment is shown in legends. Statistical significance between the groups was determined following normality test, using the Shapiro–Wilk test, and using the Student's t test. Unpaired t test with Welch's correction or one-way ANOVA with post hoc Tukey's test, as appropriate; *#p , 0.05, **p , 0.01, ***p , 0.001.

Results

ZIP1 and ZIP3 expression and Zn^{2+} transport are developmentally regulated in hippocampal neurons in vitro

We first sought to determine temporal and spatial changes in expression of ZIP1 and ZIP3 in cultured hippocampal neurons. Immunofluorescent labeling of ZIP1 or ZIP3 in young cultured hippocampal neurons (DIV12), shows that both transporters are expressed in the majority of the cells (Fig. 1A). Moreover, we detected a similar expression profile in mature hippocampal neurons (DIV21; Fig. 1B), with ZIP1 and ZIP3 expression outlining somas, Tau-positive axons and Tau-negative dendrites. Both, mature and young neurons exhibit ZIP1 immunostaining on the entirety of the cells, whereas ZIP3 signal is found primarily, but not exclusively, on neuronal somas in young neurons, extending into neuronal processes during maturation of the cells (Fig. 1A, B). qPCR analysis of young and mature neurons shows that mRNA expression levels of ZIP1 increase by 19 6 4% and ZIP3 levels increase by 48 6 8% (Fig. 1C) during in vitro maturation. To determine whether ZIP1 and ZIP3 expression levels affect neuronal Zn^{2+} accumulation, we studied transport activity in primary cultured neurons loaded with the Zn^{2+}-sensitive cytosolic fluorescent probe FluoZin-3 while transiently exposing cells to 100 mM Zn^{2+}. Rates of Zn^{2+} accumulation were increased by 46 6 12% in mature neurons compared with young cells (Fig. 1D, E). These data suggest that ZIP1 and ZIP3 are developmentally, but not differentially, expressed in primary neuronal cultures, and that both may play an important role in Zn^{2+} transport.

To distinguish between Zn^{2+} transport mediated by ZIP1 or ZIP3 in cultured neurons, we selectively silenced either ZIP1 or

ZIP3 using shRNA adeno-associated viral vectors expressing RFP as marker. We then monitored Zn^{21} accumulation using FluoZin-3 fluorescence in RFP-positive cells. Rates of Zn^{21} transport were reduced by 52 6 6% in shZIP1-expressing cells and by 45 6 6% in shZIP3-expressing cells, compared with control cells expressing a scrambled sequence (Fig. 2A, B). These values are in agreement with the reduction in Zn^{21} transport noted earlier on knock-out of both transporters (Qian et al., 2011). Unfortunately, silencing of both transporters simultaneously induced widespread neuronal cell death in the cultures, such that Zn^{21} uptake could not be assessed. This is likely the result of severe Zn^{21} deficiency (Ahn et al., 1998, 2006; Kim et al., 2015) induced by loss of both Zn^{21} importers, as well as a possible lack of compensatory mechanisms for Zn^{21} uptake in the mature neuronal culture. Next, we asked whether the expression of other neuronal Zn^{21} transporters (Lovell et al., 2005; Bosomworth et al., 2013; Leyva-Illades et al., 2014) may be affected following either ZIP1 or ZIP3 downregulation. qPCR analysis (Fig. 2C) indicated that the shZIP1 constructs resulted in silencing of 39 6 8% of ZIP1, while shZIP3 yielded 63 6 13% knock-down of ZIP3. We noted that ZnT3 mRNA levels were also reduced (35 6 4%) in ZIP3 knock-down cells. However, neither shRNA constructs significantly altered the expression of other transporters examined, namely, ZIP12, ZnT1, and ZnT10, previously linked to neuronal function (Qin et al., 2009; Bosomworth et al., 2013; Chowanadisai et al., 2013; Sindreu et al., 2014; Krall et al., 2020). These results suggest a previously unanticipated role for ZIP3 in vesicular Zn^{21} accumulation, indirectly associated with ZnT3 expression. Altogether, our data indicate that downregulation of either ZIP1 or ZIP3 expression results in decreased rates of Zn^{21} uptake that is likely not mediated by changes in expression of other transporters.

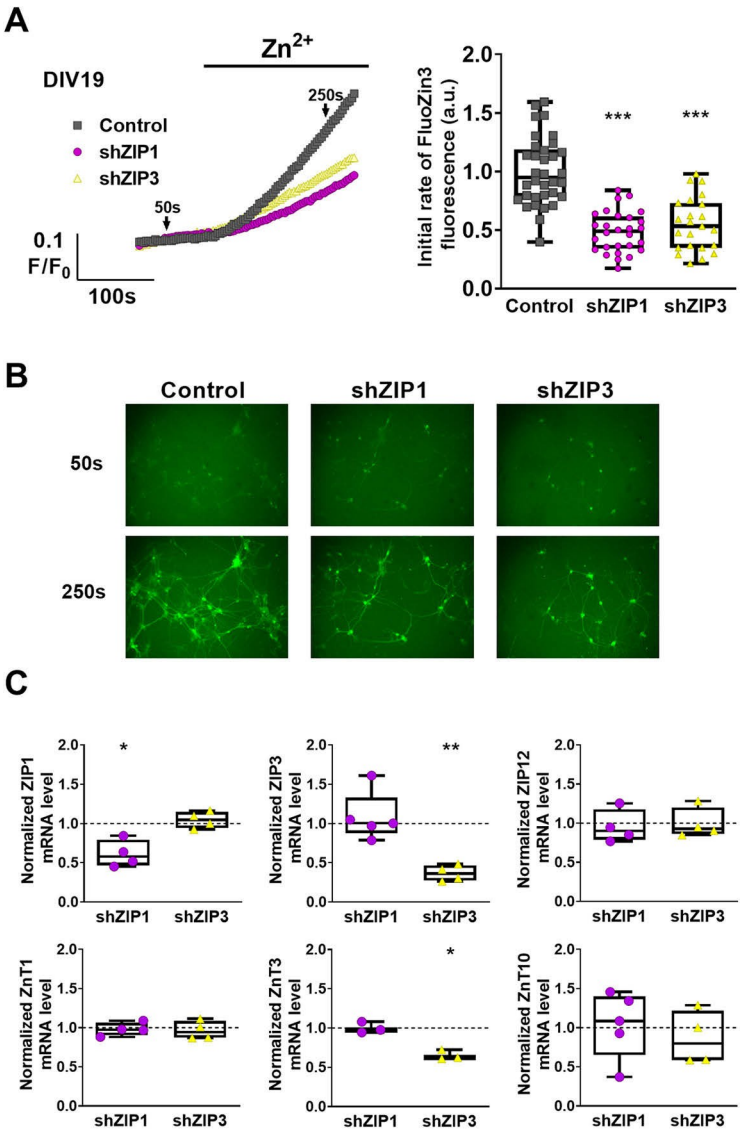

Figure 2. Silencing of ZIP1 or ZIP3 expression reduces Zn^{21} uptake in cultured hippocampal neurons. A, Traces of FluoZin-3 fluorescence increase in primary hippocampal neurons transduced with shRNA constructs to silence ZIP1 or ZIP3 (shZIP1, magenta; shZIP3, yellow) or control vector (gray). Neurons were perfused with Ringer's solution and then treated with 100 Zn^{21} at the indicated time. Right panel shows averaged initial rate of fluorescence change (n 23 coverslips per group from 6 independent experiments; **p 0.001, using ANOVA comparison relative to control cells). B, Representative images of FluoZin-3 fluorescence in primary hippocampal neurons at the time points marked by arrows in A (10 magnification). C, Analysis of mRNA expression levels of transporters in control (normalized to 1, shown as dotted line) and shRNA transduced primary hippocampal neurons for each group; *p 0.05, **p 0.01; using t test relative to control cells).

Distinct ZIP1 and ZIP3 expression and function in acute hippocampal slices

Since neurons in cultures may vary in protein expression or behavior (Dabrowski et al., 2003; Belle et al., 2018), we next evaluated the expression of ZIP1/ZIP3 in intact hippocampal tissues. We first monitored the age-dependent expression of these transporters and found that between P7 and P14 mRNA levels of ZIP1 increased by 50 6 10% (Fig. 3A) and ZIP3 mRNA levels increased by 66 6 13% (Fig. 3A). Thus, in agreement with the in vitro results, ZIP transporters expression is increased during neuronal maturation.

Next, we determined ZIP1 and ZIP3 expression pattern by immunostaining analysis in hippocampal slices. In tissues from 1- to 1.5-month-old (adult) mice (Fig. 3B), ZIP1 was predominantly expressed in stratum pyramidale, while ZIP3 fluorescent signal was mainly localized in stratum lucidum, MF-rich region near the CA3, but not in CA1 (Fig. 3C,D). Some overlap of the fluorescent signals was nonetheless observed in the interface between the MFs and the pyramidal cell layer (Fig. 3C). Consistent with ZIP3 staining of MFs, we also observed ZIP3 staining in the DG cells (Fig. 3E). Interestingly, ZIP3 expression pattern was similar to the previously observed Timm's stain of Zn^{21} in the hippocampus (Sekler et al., 2002), and to the corresponding immunostaining pattern previously observed for ZnT3 (Palmiter et al., 1996; Cole et al., 1999). This again suggests a link between ZIP3 and zincergic presynaptic neurons. To determine whether this expression pattern is developmentally regulated, we then stained tissue from 14-d-old mice (Fig. 3F,G) and neonates (P1; Fig. 3H). In hippocampal tissue from 14-d-old mice, we found clear ZIP1 and ZIP3 expression in both CA3 pyramidal cell layer and the stratum lucidum, although ZIP1 expression

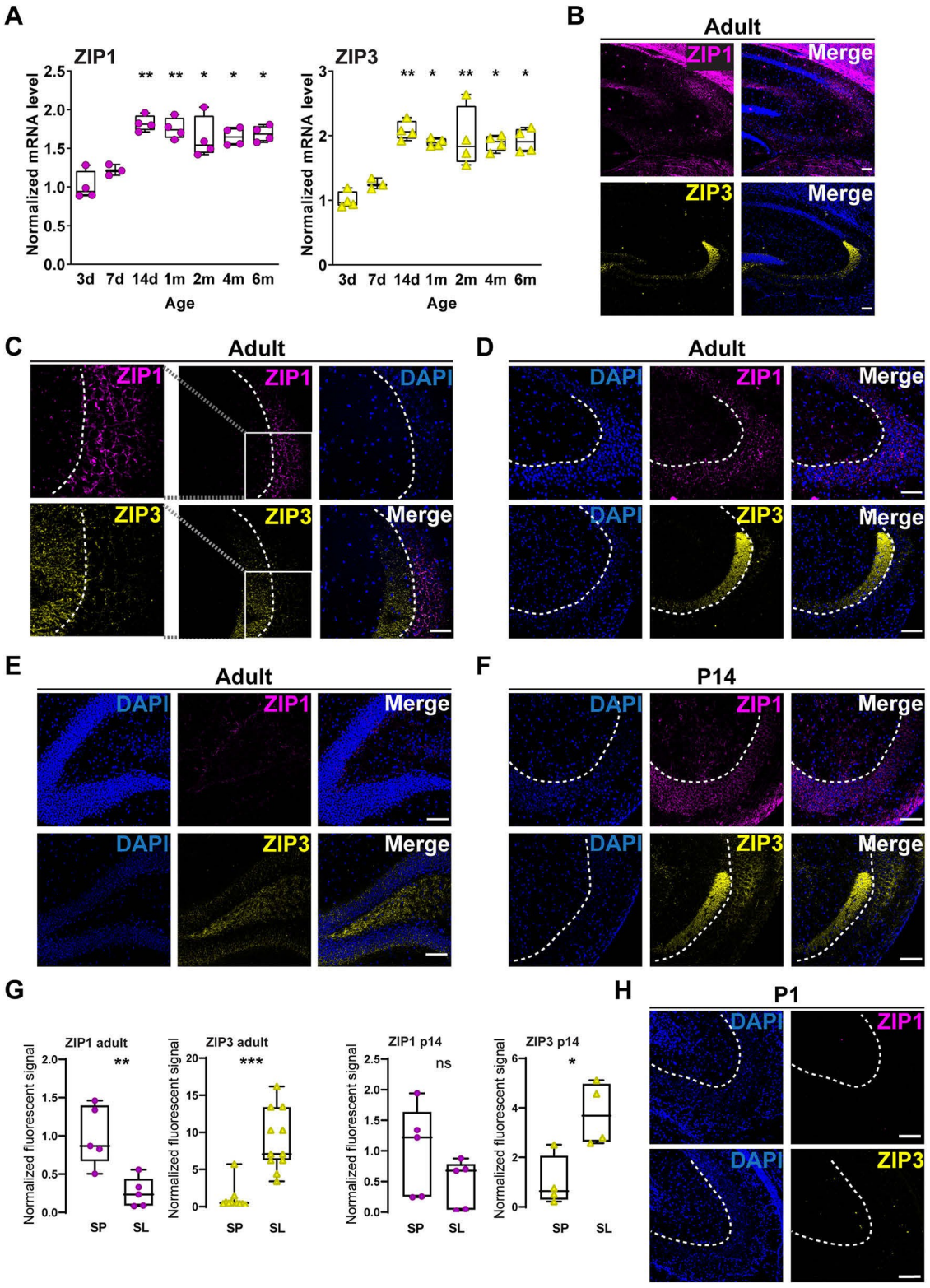

Figure 3. Developmental regulation and specific expression of ZIP1 and ZIP3 in the hippocampus. A, Comparison of mRNA levels of ZIP1 and ZI the indicated ages (*p 0.05, **p 0.01; relative to 7 d, as determined by ANOVA comparisons, n = 3–4 mice per age group). B, Representative im ZIP3 (yellow, lower panel) immunolabeling in hippocampal tissue from adult animals. Right panels are merged images with DAPI staining (10). C pocampal CA3 region, targeting ZIP1 (magenta) and ZIP3 (yellow) and co-stained with DAPI for nuclei (blue). Left panels show zoom-in of the re els are 20 images. D, ZIP1 (magenta, upper panels) and ZIP3 (yellow, lower panels) immunolabeling in hippocampal CA3 region (D) and DG (E) in tissues from one-, Similar ZIP1 and ZIP3 staining in CA3 region in 6-month-old mice. G, Normalized fluorescence of ZIP1 and ZIP3 in stratum lucidum compared with stratum pyramidale mice for each age; *p 0.05, **p 0.01, ***p 0.001; t tests, ns, non significant). H, ZIP1 and ZIP3 staining in neonatal P1 mouse tissue [dashed lines mark the borde lucidum (SL) and stratum pyramidale (SP); scale bar: 100 mm in all images].

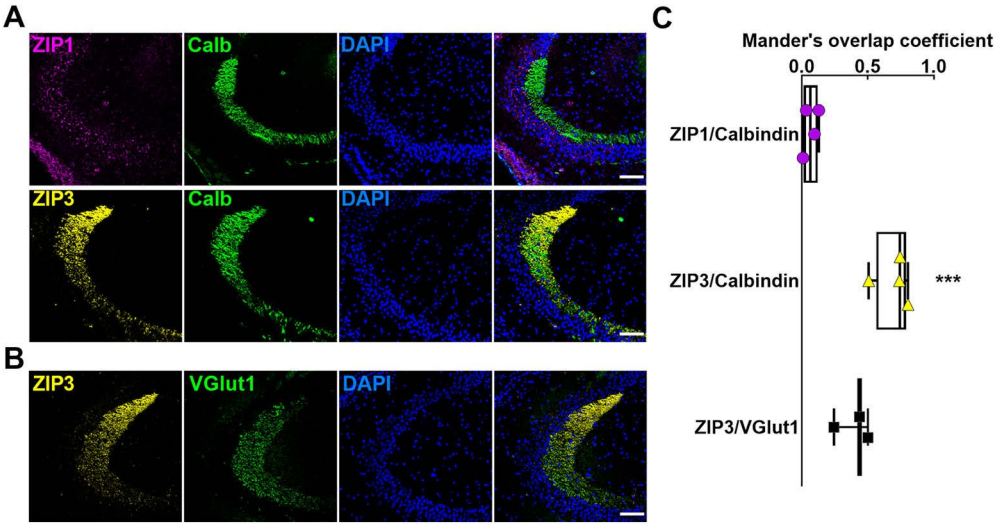

Figure 4. ZIP3 colocalizes with MF neuronal markers. A, ZIP1 (magenta, upper panels) and ZIP3 (yellow, lower panels) co-immunofluorescent lab and DAPI nuclear stain (blue). B, ZIP3 (yellow) and Vglut1 (green) co-immunofluorescent labeling. Nuclei are stained with DAPI (blue). Scale bar ficients of ZIP1 and ZIP3 with calbindin and ZIP3 with Vglut1 (n = 3–4 sections per group; ***p 0.001 compared with ZIP1/Calbindin, using t test)

tended to be higher in CA3 cells, while ZIP3 levels were slightly increased in the lucidum layer (Fig. 3G). We could not detect expression of either protein in the neonate brain (Fig. 3H), in agreement with the low mRNA expression even at P3 (Fig. 3A).

To further assess whether ZIP3 localizes to MF terminals, we performed co-immunofluorescent labeling with the MF marker calbindin (Fig. 4A). Colocalization analysis revealed that ZIP3, but not ZIP1, had strong overlap in expression pattern with that of calbindin (Fig. 4A,C). Similar overlap was observed in intensity profiles of ZIP3 and the vesicular glutamate transporter, Vglut1, suggesting that these transporters expression profiles colocalize in hippocampal tissue (Fig. 4B,C). These results suggest that in adult mouse brain, while ZIP1 is expressed on the postsynaptic CA3 neurons, ZIP3 is primarily expressed on the MFs terminals of DG neurons.

Considering the distinct expression pattern of ZIP1 and ZIP3 in the hippocampus, we next asked whether ZIP1 and ZIP3 are responsible for Zn^{21} uptake into the different ends of the MF-pyramidal cell synapses. We silenced ZIP1 or ZIP3 expression using AAV-php.EB viral vectors, containing shZIP1 or shZIP3 constructs, which had been previously delivered to the mice (see Materials and Methods). Each of the vectors also expressed RFP, which served as a marker for identifying infected cells (Fig. 5A–D). Note that RFP expression is seen in CA3 cells (Fig. 5A), and also in DG cells including the MF terminals in the CA3 lucidum layer (Fig. 5D), suggesting that numerous fibers originate from mature DG infected neurons. We then performed live tissue imaging of acute hippocampal slices with the cell permeant FluoZin-3 to measure cytosolic Zn^{21} uptake in neurons from different hippocampal subregions. In slices obtained from mice previously transduced with AAV-RFP-shZIP1, CA3 pyramidal neurons demonstrated 30 6 12% lower Zn^{21} uptake rate compared with RFP-expressing control cells (Fig. 5B). In contrast, silencing of ZIP3 did not diminish Zn^{21} uptake in the CA3 postsynaptic region (Fig. 5C). This finding is in agreement with our result showing that ZIP1, but not ZIP3, is expressed on the CA3 pyramidal cells (Fig. 3). Based on the localization of ZIP3 on the MF terminals of the DG granule cells (Figs. 3, 4), we next imaged Zn^{21} uptake in the dentate granule cells (Fig. 5D). Granule cells showed 47 6 10% decreased Zn^{21} accumulation in shZIP3 neurons compared with control RFP-expressing cells (Fig. 5E). These results, together with the specific localization of ZIP1 and ZIP3 shown in Figure 3, strongly support a distinct role for ZIP1 and ZIP3 in Zn^{21} uptake in specific neuronal populations. As such, ZIP1 is responsible for postsynaptic uptake of Zn^{21} into CA3 pyramidal cells, whereas ZIP3 mediates uptake of Zn^{21} in the presynaptic cells. To test whether silencing of ZIP3 also affects vesicular accumulation of Zn^{21} in the MFs, we loaded shZIP3 hippocampal slices with the Zn^{21}-selective dye, ZP1, which accumulates in vesicular compartments (Burdette et al., 2001). To quantify the accumulated level of Zn^{21}, we determined the difference in fluorescent signal influenced by the cell permeant Zn^{21} chelator, TPEN (40 m). which quenches ZP1 fluorescence. This difference in the fluorescent signal, TPEN (Aras et al., 2009), represents the initial level of Zn^{21} accumulated in the vesicle. We then calculated the difference of the fluorescent signal between baseline and TPEN treatment. The quenching of ZP1 fluorescence by TPEN was similar in shZIP3 and control neurons (Fig. 5F), indicating that silencing of ZIP3 does not reduce baseline vesicular Zn^{21} levels. This suggests that silencing of ZIP3 does not abolish the long-term accumulation of Zn^{21} in synaptic vesicles, at least within the timeframe of these experiments.

Silencing of ZIP3, but not ZIP1, prevents seizure-dependent CA3 pyramidal cells neurodegeneration

We next sought to determine the individual contributions of ZIP1 and ZIP3 to neuronal injury following kainate-induced seizures, as the concomitant loss of both transporters together has previously been shown to be neuroprotective (Qian et al., 2011). Mice were infected with either shZIP1 or shZIP3 using the viral vectors, as described above, and seven weeks later, mice were injected intraperitoneally with 25–30 mg/kg kainic acid to induce epileptic seizures, as described previously (Tse et al., 2014). We analyzed neuronal degeneration in the CA3 region only in mice that showed grade 5 seizure (continuous rearing and loss of posture) that was maintained for 30 min (see Materials and Methods). In hippocampal tissues obtained from the mice 24 h after seizure (see Materials and Methods),

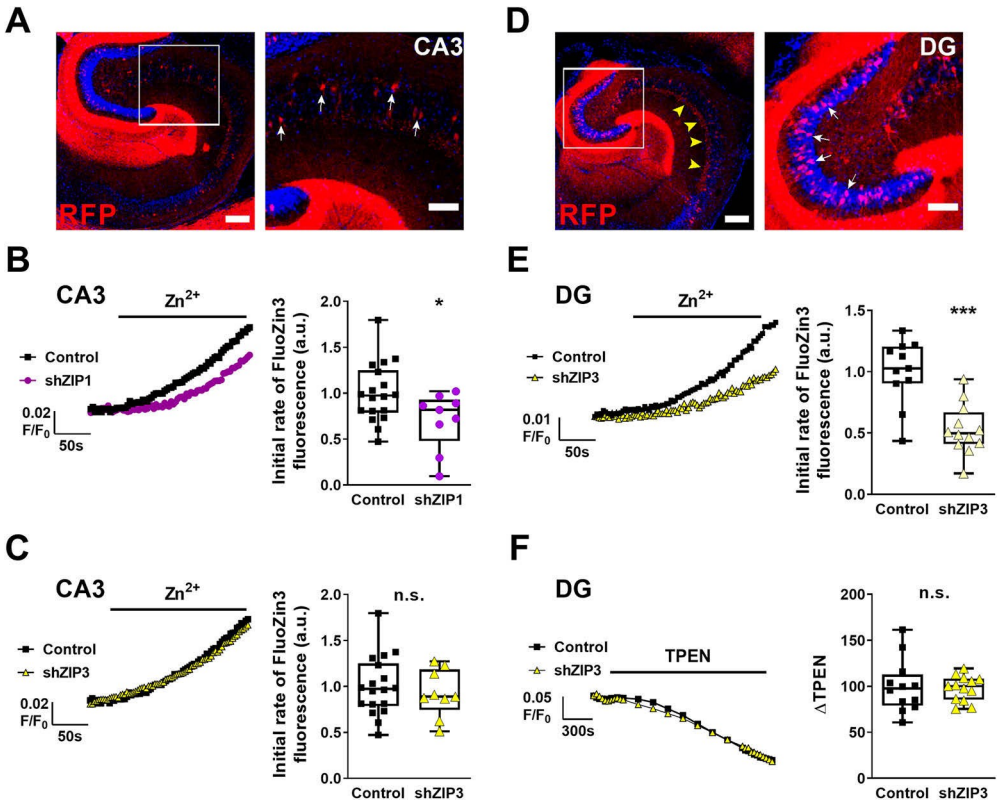

Figure 5. ZIP1 and ZIP3 are mediating Zn^{2+} uptake in distinct neuronal populations in hippocampus. *A*, Representative fluorescent images of acute hippocampal slices from mice transduced with AAV-RFP-shRNA-ZIP1 knockdown ZIP1 expression and stained with nuclear (DAPI). Left panel shows the whole hippocampus (scale bar: 250 mm), with CA3 region marked by box. Right panel shows a zoom-in of the CA3 region (scale bar: 100 mm). RFP-positive CA3 pyramidal neurons (e.g., white arrows in right panel) express the silencing construct. *B*, *C*, Matching slices were loaded with FluoZin-3, and Zn^{2+} transport in RFP-positive cells was monitored. Representative traces show FluoZin-3 fluorescence from slices transduced with shZIP1 (yellow trace) or control vector (black trace) in left panels. Averaged initial slope quantification of Zn^{2+} accumulation in CA3 pyramidal neurons is shown in the corresponding right panels. *D*, Representative fluorescent images of acute slices transduced with AAV-RFP-shRNA vectors aimed at knockdown of ZIP3 (red). Left panel shows the whole hippocampus (scale bar, 250 mm), with DG marked in box. Note expression of RFP fluorescence in the stratum lucidum of CA3 (yellow arrows, right panel) is a zoom-in on the DG cells (scale bar, 100 mm). RFP-positive DG granule cells express the silencing construct (e.g., white arrows in right panel). *E*, FluoZin-3 fluorescent signals were monitored in RFP-positive cells expressing shZIP3 (yellow trace) or control vector (black trace). Representative traces are shown in the left panel, and averaged initial slope quantification of Zn^{2+} accumulation in DG granule neurons is shown in the corresponding right panel. *F*, Slices from shZIP3 transduced animals were loaded with the sensitive dye FluoZin-3, and baseline fluorescent signals was acquired and the Zn^{2+} chelator TPEN (50 mM) was added as marked. Representative traces are shown in the left panel, and averaged difference between baseline fluorescent signal and the signal at 30 min following application of TPEN, (DTPEN), is shown in the right panel (*p 0.05, ***p 0.001, n.s.: non significant, using t test; n = 9–12 hippocampal slices from 3 animals for each group).

Nissl staining revealed apoptotic bodies and neuronal degeneration throughout the CA3 pyramidal layer in all control animals (Fig. 6A, Top panels) and in animals transduced with AAV-RFP-shZIP1 (Fig. 6A, central panels). In contrast, neuronal loss was markedly reduced in AAV-RFP-shZIP3 transduced animals (Fig. 6A, bottom panels) compared with controls or to shZIP1 transduced animals. This reduction in neuronal loss was evident despite the fact that grade 5 seizures were still present in these animals. To quantify neuronal degeneration, we used Fluor-Jade B (FJ) staining, which marks injured cells. In the CA3 region of AAV-RFP-shZIP3 transduced animals, we monitored 54 6 18% less FJ^1 (Fluoro-Jade B positive) cells compared with control animals (Fig. 6B,C). Moreover, shZIP3 tissue contained 63 6 14% fewer FJ^1 cells compared with AAV-RFP-shZIP1 transduced animals. Finally, silencing of ZIP1 using the shZIP1 construct did not show any protection from kainic acid induced neurotoxicity, and numbers of FJ^1 cells were similar to the control group (Fig. 6B,C). Taken together, these results suggest that ZIP3, but not ZIP1, has a critical role in kainate neurotoxicity of CA3 pyramidal cells.

Discussion

Expression of Zn^{21} transporters is upregulated during the first postnatal weeks, together with multiple proteins (Slomianka and Geneser, 1997), but can also be modulated by Zn^{21} availability (Liuzzi et al., 2001; Nitzan et al., 2002; Sekler et al., 2002; Huang et al., 2006). We observe significant upregulation of ZIP1 and ZIP3 expression that is paralleled by increased rates of neuronal Zn^{21} influx in hippocampal neurons during the first two weeks in vitro. In acute hippocampal tissue sections, neither transporter was detectable at the first postnatal day, but by two weeks of age, we find marked expression of both proteins in the CA3 pyramidal cell layer as well as in the stratum lucidum. This increased expression of ZIP1 and ZIP3 is concomitant with increased synaptic Zn^{21} concentrations in CA3 hippocampal region (Nitzan et al., 2004; McAllister and Dyck, 2017), suggests that there may be developmental homeostatic regulation of ZIP1 and ZIP3 expression and Zn^{21} accumulation. Surprisingly, we observed that in the adult hippocampus (1–1.5 months) the transporters are expressed in distinct regions, with ZIP1 primarily localized to the stratum pyramidale of the CA3 and ZIP3 mainly present in the dentate granule cells and the MFs extending from them

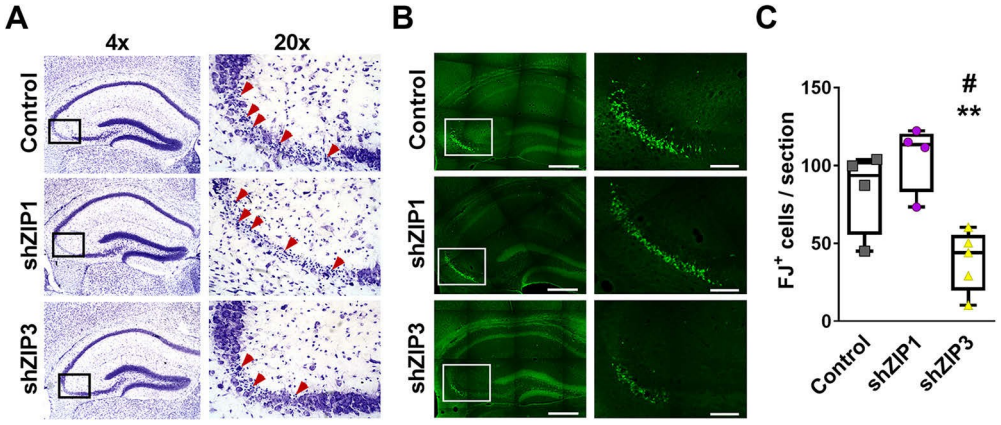

Figure 6. Silencing of hippocampal ZIP3 expression prevents seizure-induced neurodegeneration of CA3 pyramidal neurons. A, Representative low (4× panel) and high (20× panel) magnification micrographs of Nissl staining showing neurodegeneration in the CA3 pyramidal layer, 24 h following kainic acid administratio transduced with shRNA-RFP-AAV control empty vectors (top panels) or vectors aimed to silence ZIP1 (middle panels) or ZIP3 (bottom panels). A recognized. B, Adjacent sections (to those presented in A) were stained with Fluoro-Jade B (green) marking degenerating neurons. Representati fication images are shown, as in A. Scale bar: 400 mm in 4 and 100 mm in 20. C, Quantification of FJ+ cells (n = 4 mice for control and shZIP1, n = 5 mic #p 0.05 compared with control; **p 0.01 compared with shZIP1, using ANOVA).

into the stratum lucidum. Since ZIP3 mRNA is similarly expressed in both strata (Allen Mouse Brain Atlas, 2004), we suggest that ZIP3 protein expression may be tightly regulated by the accumulated Zn^{2+} that is found in the MF terminals together with ZnT3 (Palmiter et al., 1996; Wenzel et al., 1997). Importantly, the specific expression pattern of ZIP1 and ZIP3 agrees with our findings that the activity of the transporters affects Zn^{2+} accumulation in distinct strata of the hippocampus. Accordingly, silencing of ZIP1 reduced Zn^{2+} accumulation in CA3 neurons, while ZIP3 silencing reduced Zn^{2+} accumulation in DG cells. These findings support our hypothesis that ZIP1 and ZIP3 have distinct roles in regulating Zn^{2+} during neuronal activity.

Expression of ZIP3 follows the pattern of the glutamate transporter 1 expression, suggesting that ZIP3 is in close proximity to glutamatergic vesicles-containing synaptic terminals, similar to the ZnT3 expression pattern (Salazar et al., 2005; McAllister and Dyck, 2017). Thus, we suggest that ZIP3-mediated influx of Zn^{2+} into the dentate granule cells is important for re-uptake and re-packaging of Zn^{2+} previously released from the MFs. Interestingly, transient silencing of ZIP3 in hippocampal cultures induced a decrease in ZnT3 expression, suggesting that ZIP3 and ZnT3 transporter function may be coordinated to regulate Zn^{2+} homeostasis. In contrast, we did not see a decrease in the synaptic Zn^{2+} pools in the DG cells following ZIP3 silencing in vivo. This indicates that although rapid Zn^{2+} influx and re-uptake is attenuated in the dentate granule cells by ZIP3 silencing, the long-term accumulation of vesicular Zn^{2+} (at least within the timeframe studied here) is maintained even in the absence of ZIP3. Such uptake can be mediated by numerous Zn^{2+} transporting proteins, which may be upregulated during the development of shZIP3 mice that were infected at P1. In contrast, in primary neuronal cultures silencing was performed only on day 10, when the neurons are relatively differentiated (Ichikawa et al., 1993) and therefore adaptation of Zn^{2+} re-uptake mechanisms may be less likely to appear. Indeed, silencing both ZIP1 and ZIP3 in the cultured neurons resulted in massive cell death, likely as a result of severe Zn^{2+} deficiency in the absence of the compensatory re-uptake mechanisms. Clearly, additional studies are needed to further characterize the complex regulation of Zn^{2+} present in synaptic terminals.

Here, we describe specific localization of ZIP1 and ZIP3 and their distinct roles in Zn^{2+} accumulation, suggesting that these transporters play different roles in Zn^{2+}-related neurotoxicity in the CA3 region of the hippocampus. Surprisingly, we found that silencing of the postsynaptic ZIP1 had no effect on survival of CA3 neurons, suggesting that the influx mediated by this transporter is not a main route for Zn^{2+} entry into postsynaptic neurons during excitotoxic conditions. In fact, previous studies suggested that excitotoxicity-induced neuronal Zn^{2+} translocation into postsynaptic cells is primarily mediated by Ca^{2+}-permeable AMPA channels and voltage gated Ca^{2+} channels (Sensi et al., 1999; Jia et al., 2002; Takeda et al., 2009; Medvedeva et al., 2017; Ji and Weiss, 2018). Another important mechanism for Zn^{2+} toxicity is via intracellular liberation in the postsynaptic cells (Aizenman et al., 2000) which is also likely independent of ZIP1. Thus, our results further indicate that ZIP1-dependent Zn^{2+} permeation is not a major player in neuronal death in excitotoxic conditions. Nonetheless, the precise physiological role for this transporter remains to be established.

In contrast to the effect of ZIP1 silencing, knock-down of ZIP3 resulted in attenuated CA3 neuronal death, suggesting that regulation of presynaptic Zn^{2+} uptake is critically important for neuronal survival during excitotoxic conditions. What possible mechanism may account for this observation? For one, loss of ZIP3 from the presynaptic MF terminals, and possible decreased re-uptake may promote activation of mechanisms shown previously to decrease synaptic glutamatergic excitation in the postsynaptic cells. For example, we previously demonstrated that transient changes in extracellular Zn^{2+} activate mZnR/GPR39 signaling and lead to enhanced inhibition via up-regulation of the potassium/chloride co-transporter KCC2 in postsynaptic cells (Besser et al., 2009; Chorin et al., 2011). Moreover, mZnR/GPR39 activation also induces postsynaptic production and release of the endocannabinoid 2-arachidonoyl-glycerol, which, in turn, leads to a subsequent decrease in presynaptic glutamate release (Perez-Rosello et al., 2013). Alternatively, the exposure of postsynaptic neurons to increased levels of Zn^{2+}, because of diminished re-uptake in the absence of ZIP3, may eventually lead to sub-lethal Zn^{2+} permeation into postsynaptic neurons. This, in turn, may trigger activation of adaptive neuroprotective processes, including increased expression of

metallothionein (Aras et al., 2009). Buffering of Zn^{21} by MT-III in the postsynaptic cells has been suggested to protect CA3 neurons from ischemia induced cell death (Medvedeva et al., 2017). Interestingly, such an adaptive mechanism may, in fact, require ZIP1 activity in postsynaptic CA3 neurons. Indeed, in the absence of both ZIP1 and ZIP3 postsynaptic CA3 neurons are not protected from seizure damage, in contrast to CA1 neurons (Qian et al., 2011), suggesting that the adaptive rescue mechanism activated by ZIP3 silencing in CA3 neurons cannot be triggered without ZIP1-dependent Zn^{21} influx. Our results thus strongly point to critical, novel avenues to pursue in the regulation of neuronal cell death processes via modulation of specific Zn^{21} transporter function.

References

Ahn YH, Kim YH, Hong SH, Koh JY (1998) Depletion of intracellular zinc induces protein synthesis-dependent neuronal apoptosis in mouse cortical culture. Exp Neurol 154:47–56.

Ahn YH, Koh JY, Hong SH (2000) Protein synthesis-dependent but Bcl-2-independent cytochrome C release in zinc depletion-induced neuronal apoptosis. J Neurosci Res 61:508–514.

Aizenman E, Loring RH, Reynolds IJ, Rosenberg PA (2020) The redox biology of excitotoxic processes: the NMDA receptor, TOPA quinone, and the oxidative liberation of intracellular zinc. Front Neurosci 14:778.

Aizenman E, Stout AK, Hartnett KA, Dineley KE, McLaughlin B, Reynolds IJ (2000) Induction of neuronal apoptosis by thiol oxidation: putative role of intracellular zinc release. J Neurochem 75:1878–1888.

Allen Institute for Brain Science (2004) Allen Mouse Brain Atlas [experiment 2619]. Available from mouse.brain-map.org. Allen Institute for Brain Science (2011).

Anderson CT, Radford RJ, Zastrow ML, Zhang DY, Apfel UP, Lippard SJ, Tzounopoulos T (2015) Modulation of extrasynaptic NMDA receptors by synaptic and tonic zinc. Proc Natl Acad Sci USA 112:E2705–E2714.

Aras MA, Hara H, Hartnett KA, Kandler K, Aizenman E (2009) Protein kinase C regulation of neuronal zinc signaling mediates survival during preconditioning. J Neurochem 110:106–117.

Belle AM, Enright HA, Sales AP, Kulp K, Osburn J, Kuhn EA, Fischer NO, Wheeler EK (2018) Evaluation of in vitro neuronal platforms as surrogates for in vivo whole brain systems. Sci Rep 8:10820.

Belloni-Olivi L, Marshall C, Laal B, Andrews GK, Bressler J (2009) Localization of zip1 and zip4 mRNA in the adult rat brain. J Neurosci Res 87:3221–3230.

Besser L, Chorin E, Sekler I, Silverman WF, Atkin S, Russell JT, Hershfinkel M (2009) Synaptically released zinc triggers metabotropic signaling via a zinc-sensing receptor in the hippocampus. J Neurosci 29:2890–2901.

Bosomworth HJ, Adlard PA, Ford D, Valentine RA (2013) Altered expression of ZnT10 in Alzheimer's disease brain. PLoS One 8:e65475.

Burdette SC, Walkup GK, Spingler B, Tsien RY, Lippard SJ (2001) Fluorescent sensors for Zn(21) based on a fluorescein platform: synthesis, properties and intracellular distribution. J Am Chem Soc 123:7831–7841.

Challis RC, Ravindra Kumar S, Chan KY, Challis C, Beadle K, Jang MJ, Kim HM, Rajendran PS, Tompkins JD, Shivkumar K, Deverman BE, Gradinaru V (2019) Systemic AAV vectors for widespread and targeted gene delivery in rodents. Nat Protoc 14:379–414.

Chorin E, Vinograd O, Fleidervish I, Gilad D, Herrmann S, Sekler I, Aizenman E, Hershfinkel M (2011) Upregulation of KCC2 activity by zinc-mediated neurotransmission via the mZnR/GPR39 receptor. J Neurosci 31:12916–12926.

Chowanadisai W, Graham DM, Keen CL, Rucker RB, Messerli MA (2013) Neurulation and neurite extension require the zinc transporter ZIP12 (slc39a12). Proc Natl Acad Sci USA 110:9903–9908.

Cole TB, Wenzel HJ, Kafer KE, Schwartzkroin PA, Palmiter RD (1999) Elimination of zinc from synaptic vesicles in the intact mouse brain by disruption of the ZnT3 gene. Proc Natl Acad Sci USA 96:1716–1721.

Dabrowski M, Aerts S, Van Hummelen P, Craessaerts K, De Moor B, Annaert W, Moreau Y, De Strooper B (2003) Gene profiling of hippocampal neuronal culture. J Neurochem 85:1279–1288.

Dufner-Beattie J, Huang ZL, Geiser J, Xu W, Andrews GK (2005) Generation and characterization of mice lacking the zinc uptake transporter ZIP3. Mol Cell Biol 25:5607–5615.

Frederickson CJ, Danscher G (1990) Zinc-containing neurons in hippocampus and related CNS structures. Prog Brain Res 83:71–84.

Frederickson CJ, Howell GA, Frederickson MH (1981) Zinc dithizonate staining in the cat hippocampus: relationship to the mossy-fiber neuropil and postnatal development. Exp Neurol 73:812–823.

Frederickson CJ, Rampy BA, Reamy-Rampy S, Howell GA (1992) Distribution of histochemically reactive zinc in the forebrain of the rat. J Chem Neuroanat 5:521–530.

Gaither LA, Eide DJ (2001) Eukaryotic zinc transporters and their regulation. Biometals 14:251–270.

Ganay T, Asraf H, Aizenman E, Bogdanovic M, Sekler I, Hershfinkel M (2015) Regulation of neuronal pH by the metabotropic Zn(21)-sensing Gq-coupled receptor, mZnR/GPR39. J Neurochem 135:897–907.

Gee KR, Zhou ZL, Ton-That D, Sensi SL, Weiss JH (2002) Measuring zinc in living cells. A new generation of sensitive and selective fluorescent probes. Cell Calcium 31:245–251.

Gilad D, Shorer S, Ketzef M, Friedman A, Sekler I, Aizenman E, Hershfinkel M (2015) Homeostatic regulation of KCC2 activity by the zinc receptor mZnR/GPR39 during seizures. Neurobiol Dis 81:4–13.

Granzotto A, Canzoniero LMT, Sensi SL (2020) A neurotoxic ménage-à-trois: glutamate, calcium, and zinc in the excitotoxic cascade. Front Mol Neurosci 13:600089.

Groh A, de Kock CP, Wimmer VC, Sakmann B, Kuner T (2008) Driver or coincidence detector: modal switch of a corticothalamic giant synapse controlled by spontaneous activity and short-term depression. J Neurosci 28:9652–9663.

Huang ZL, Dufner-Beattie J, Andrews GK (2006) Expression and regulation of SLC39A family zinc transporters in the developing mouse intestine. Dev Biol 295:571–579.

Ichikawa M, Muramoto K, Kobayashi K, Kawahara M, Kuroda Y (1993) Formation and maturation of synapses in primary cultures of rat cerebral cortical cells: an electron microscopic study. Neurosci Res 16:95–103.

Ji SG, Weiss JH (2018) Zn(21)-induced disruption of neuronal mitochondrial function: synergism with Ca(21), critical dependence upon cytosolic Zn(21) buffering, and contributions to neuronal injury. Exp Neurol 302:181–195.

Ji SG, Medvedeva YV, Wang HL, Yin HZ, Weiss JH (2019) Mitochondrial Zn(21) accumulation: a potential trigger of hippocampal ischemic injury. Neuroscientist 25:126–138.

Jia Y, Jeng JM, Sensi SL, Weiss JH (2002) Zn21 currents are mediated by calcium-permeable AMPA/kainate channels in cultured murine hippocampal neurones. J Physiol 543:35–48.

Kalappa BI, Anderson CT, Goldberg JM, Lippard SJ, Tzounopoulos T (2015) AMPA receptor inhibition by synaptically released zinc. Proc Natl Acad Sci USA 112:15749–15754.

Kambe T, Tsuji T, Hashimoto A, Itsumura N (2015) The physiological, biochemical, and molecular roles of zinc transporters in zinc homeostasis and metabolism. Physiol Rev 95:749–784.

Kim JY, Grunke SD, Levites Y, Golde TE, Jankowsky JL (2014) Intracerebroventricular viral injection of the neonatal mouse brain for persistent and widespread neuronal transduction. J Vis Exp 15:51863.

Kim HL, Ra H, Kim KR, Lee JM, Im H, Kim YH (2015) Poly(ADP-ribosyl)ation of p53 contributes to TPEN-induced neuronal apoptosis. Mol Cells 38:312–317.

Krall RF, Moutal A, Phillips MB, Asraf H, Johnson JW, Khanna R, Hershfinkel M, Aizenman E, Tzounopoulos T (2020) Synaptic zinc inhibition of NMDA receptors depends on the association of GluN2A with the zinc transporter ZnT1. Sci Adv 6:eabb1515.

Krall RF, Tzounopoulos T, Aizenman E (2021) The function and regulation of zinc in the brain. Neuroscience 457:235–258.

Krężel A, Maret W (2021) The bioinorganic chemistry of mammalian metallothioneins. Chem Rev 121:14594–14648.

Leyva-Illades D, Chen P, Zogzas CE, Hutchens S, Mercado JM, Swaim CD, Morrisett RA, Bowman AB, Aschner M, Mukhopadhyay S (2014) SLC30A10 is a cell surface-localized manganese efflux transporter, and parkinsonism-causing mutations block its intracellular trafficking and efflux activity. J Neurosci 34:14079–14095.

Liuzzi JP, Blanchard RK, Cousins RJ (2001) Differential regulation of zinc transporter 1, 2, and 4 mRNA expression by dietary zinc in rats. J Nutr 131:46–52.

Lovell MA, Smith JL, Xiong S, Markesbery WR (2005) Alterations in zinc transporter protein-1 (ZnT-1) in the brain of subjects with mild cognitive impairment, early, and late-stage Alzheimer's disease. Neurotox Res 7:265–271.

McAllister BB, Dyck RH (2017) Zinc transporter 3 (ZnT3) and vesicular zinc in central nervous system function. Neurosci Biobehav Rev 80:329–350.

McKhann GM 2nd, Wenzel HJ, Robbins CA, Sosunov AA, Schwartzkroin PA (2003) Mouse strain differences in kainic acid sensitivity, seizure behavior, mortality, and hippocampal pathology. Neuroscience 122:551–561.

McLin JP, Steward O (2006) Comparison of seizure phenotype and neurodegeneration induced by systemic kainic acid in inbred, outbred, and hybrid mouse strains. Eur J Neurosci 24:2191–2202.

Medvedeva YV, Ji SG, Yin HZ, Weiss JH (2017) Differential vulnerability of CA1 versus CA3 pyramidal neurons after ischemia: possible relationship to sources of Zn21 accumulation and its entry into and prolonged effects on mitochondria. J Neurosci 37:726–737.

Milon B, Dhermy D, Pountney D, Bourgeois M, Beaumont C (2001) Differential subcellular localization of hZip1 in adherent and non-adherent cells. FEBS Lett 507:241–246.

Nishikawa M, Mori H, Hara M (2017) Analysis of ZIP (Zrt-, Irt-related protein) transporter gene expression in murine neural stem/progenitor cells. Environ Toxicol Pharmacol 53:81–88.

Nitzan YB, Sekler I, Hershfinkel M, Moran A, Silverman WF (2002) Postnatal regulation of ZnT-1 expression in the mouse brain. Brain Res Dev Brain Res 137:149–157.

Nitzan YB, Sekler I, Silverman WF (2004) Histochemical and histofluorescence tracing of chelatable zinc in the developing mouse. J Histochem Cytochem 52:529–539.

Palmiter RD, Cole TB, Quaife CJ, Findley SD (1996) ZnT-3, a putative transporter of zinc into synaptic vesicles. Proc Natl Acad Sci USA 93:14934–14939.

Perez-Rosello T, Anderson CT, Schopfer FJ, Zhao Y, Gilad D, Salvatore SR, Freeman BA, Hershfinkel M, Aizenman E, Tzounopoulos T (2013) Synaptic Zn21 inhibits neurotransmitter release by promoting endocannabinoid synthesis. J Neurosci 33:9259–9272.

Qian J, Xu K, Yoo J, Chen TT, Andrews G, Noebels JL (2011) Knockout of Zn transporters Zip-1 and Zip-3 attenuates seizure-induced CA1 neurodegeneration. J Neurosci 31:97–104.

Qin Y, Thomas D, Fontaine CP, Colvin RA (2009) Silencing of ZnT1 reduces Zn21 efflux in cultured cortical neurons. Neurosci Lett 450:206–210.

Saadi RA, He K, Hartnett KA, Kandler K, Hershfinkel M, Aizenman E (2012) SNARE-dependent upregulation of potassium chloride co-transporter 2 activity after metabotropic zinc receptor activation in rat cortical neurons in vitro. Neuroscience 210:38–46.

Salazar G, Craige B, Love R, Kalman D, Faundez V (2005) Vglut1 and ZnT3 co-targeting mechanisms regulate vesicular zinc stores in PC12 cells. J Cell Sci 118:1911–1921.

Schauwecker PE (2003) Genetic basis of kainate-induced excitotoxicity in mice: phenotypic modulation of seizure-induced cell death. Epilepsy Res 55:201–210.

Schauwecker PE, Steward O (1997) Genetic determinants of susceptibility to excitotoxic cell death: implications for gene targeting approaches. Proc Natl Acad Sci USA 94:4103–4108.

Schauwecker PE, Wood RI, Lorenzana A (2009) Neuroprotection against excitotoxic brain injury in mice after ovarian steroid depletion. Brain Res 1265:37–46.

Sekler I, Moran A, Hershfinkel M, Dori A, Margulis A, Birenzweig N, Nitzan Y, Silverman WF (2002) Distribution of the zinc transporter ZnT-1 in comparison with chelatable zinc in the mouse brain. J Comp Neurol 447:201–209.

Sensi SL, Yin HZ, Carriedo SG, Rao SS, Weiss JH (1999) Preferential Zn21 influx through Ca21-permeable AMPA/kainate channels triggers prolonged mitochondrial superoxide production. Proc Natl Acad Sci USA 96:24142419.

Sensi SL, Paoletti P, Koh JY, Aizenman E, Bush AI, Hershfinkel M (2011) The neurophysiology and pathology of brain zinc. J Neurosci 31:16076–16085.

Sindreu C, Bayés Á, Altafaj X, Pérez-Clausell J (2014) Zinc transporter-1 concentrates at the postsynaptic density of hippocampal synapses. Mol Brain 7:16.

Slomianka L, Geneser FA (1997) Postnatal development of zinc-containing cells and neuropil in the hippocampal region of the mouse. Hippocampus 7:321–340.

Styrpejko DJ, Cuajungco MP (2021) Transmembrane 163 (TMEM163) protein: a new member of the zinc efflux transporter family. Biomedicines 9:220.

Takeda A, Sakurada N, Ando M, Kanno S, Oku N (2009) Facilitation of zinc influx via AMPA/kainate receptor activation in the hippocampus. Neurochem Int 55:376–382.

Tse K, Puttachary S, Beamer E, Sills GJ, Thippeswamy T (2014) Advantages of repeated low dose against single high dose of kainate in C57BL/6J mouse model of status epilepticus: behavioral and electroencephalographic studies. PLoS One 9:e96622.

Tzeng TT, Tsay HJ, Chang L, Hsu CL, Lai TH, Huang FL, Shiao YJ (2013) Caspase 3 involves in neuroplasticity, microglial activation and neurogenesis in the mice hippocampus after intracerebral injection of kainic acid. J Biomed Sci 20:90.

Weiss JH, Sensi SL (2000) Ca21-Zn21 permeable AMPA or kainate receptors: possible key factors in selective neurodegeneration. Trends Neurosci 23:365–371.

Wenzel HJ, Cole TB, Born DE, Schwartzkroin PA, Palmiter RD (1997) Ultrastructural localization of zinc transporter-3 (ZnT-3) to synaptic vesicle membranes within mossy fiber boutons in the hippocampus of mouse and monkey. Proc Natl Acad Sci USA 94:12676–12681.

Woodroofe CC, Masalha R, Barnes KR, Frederickson CJ, Lippard SJ (2004) Membrane-permeable and -impermeable sensors of the Zinpyr family and their application to imaging of hippocampal zinc in vivo. Chem Biol 11:1659–1666.

Zhang Y, Wang H, Li J, Jimenez DA, Levitan ES, Aizenman E, Rosenberg PA (2004) Peroxynitrite-induced neuronal apoptosis is mediated by intracellular zinc release and 12-lipoxygenase activation. J Neurosci 24:10616–10627.

Zhang Y, Aizenman E, DeFranco DB, Rosenberg PA (2007) Intracellular zinc release, 12-lipoxygenase activation and MAPK dependent neuronal and oligodendroglial death. Mol Med 13:350–355.